Reduction in CD11c$^+$ microglia correlates with clinical progression in chronic experimental autoimmune demyelination

Florian Mayrhofer[b], Zhanna Dariychuk[b], Anthony Zhen[b], Daniel J. Daugherty[a,b], Peter Bannerman[b], Angela M. Hanson[b], David Pleasure[b], Athena Soulika[b], Wenbin Deng[a,b], Olga V. Chechneva[a,b*]

[a]Department of Biochemistry and Molecular Medicine, UC Davis, Sacramento, CA 95817;
[b]IPRM, Shriners Hospital for Children, Sacramento, CA 95817

Corresponding author: ochechneva@ucdavis.edu

Abstract

Multiple sclerosis (MS) is a chronic autoimmune demyelinating disease with high variability of clinical symptoms. In most cases MS appears as a relapsing-remitting disease course that at a later stage transitions into irreversible progressive decline of neurologic function. The mechanisms underlying MS progression remain poorly understood. Experimental autoimmune encephalomyelitis (EAE) is an animal model of MS. Here we demonstrate that mice that develop mild EAE after immunization with myelin oligodendrocyte glycoprotein 35-55 are prone to undergo clinical progression around 30 days after EAE induction. EAE progression was associated with reduction in CD11c$^+$ microglia and dispersed coalescent parenchymal infiltration. We found sex-dependent differences mediated by p38α signaling, a key regulator of inflammation. Selective reduction of CD11c$^+$ microglia in female mice with CD11c-promoter driven *p38α* knockout (*KO)* correlated with increased rate of EAE progression. In protected animals, we found CD11c$^+$ microglia forming contacts with astrocyte processes at the glia limitans and immune cells retained within perivascular spaces. Together, our study provides evidence on the protective role of CD11c$^+$ microglia in controlling CNS immune cell parenchymal infiltration in autoimmune demyelination.

Keywords: CD11c$^+$ microglia, EAE progression, CNS infiltration, p38α sexual dimorphism, glia limitans

Introduction

Multiple sclerosis (MS) is an autoimmune demyelinating disorder characterized by myelin loss, chronic inflammation, and axonal degeneration. MS is a complex disease with variable outcomes. In 80% of patients, MS appears as a relapsing-remitting form (RRMS), where episodes of neurologic dysfunction are separated by periods of remission (Baecher-Allan et al., 2018). Within a decade of first diagnosis, the majority of RRMS patients develop progression of clinical deficits (Coret et al., 2018; Zhang et al., 2015). The progressive form of MS is refractory to approved RRMS disease-modifying therapies and mechanisms of clinical progression in MS are poorly understood (Goldschmidt and McGinley, 2021).

CD11c$^+$ microglia are unique microglia that emerge in the CNS during development and injury (Butovsky et al., 2006; Hagemeyer et al., 2017; Kamphuis et al., 2016; Wlodarczyk et al., 2015; Wlodarczyk et al., 2017). CD11c$^+$ microglia have poor antigen presenting capacity (Ford et al., 1995; Giles et al., 2018; Greter et al., 2005; Miller et al., 2007) and increase in CD11c$^+$ microglia precedes the onset of experimental autoimmune encephalomyelitis (EAE) an animal model of MS (Fischer and Reichmann, 2001; Serafini et al., 2000). A growing number of evidences suggests that CD11c$^+$ microglia possess a neuroprotective function in disease. Increase in CD11c$^+$ microglia reduced clinical disability in EAE (Wlodarczyk et al., 2018) and alleviated cuprizone-induced demyelination (Sato-Hashimoto et al., 2019). CD11c$^+$ microglia were identified on site of amyloid plaques preventing plaque formation in a transgenic model of Alzheimer's disease (Butovsky et al., 2006; Kamphuis et al., 2016; Keren-Shaul et al., 2017). The function of CD11c$^+$ microglia in autoimmune demyelination is not well understood.

Among the key regulators of inflammation is mitogen-activated protein kinase (MAPK) 14 or p38α (Zarubin and Han, 2005). p38α expression is upregulated in active and chronic lesions in patients with MS (Lock et al., 2002). p38α signaling in CD11c$^+$ classical dendritic

56 cells (cDC) is required for the differentiation of uncommitted T cells toward T_H17 phenotype
57 in MS and EAE and involves the IL-6 – STAT3 signaling pathway (Di Mitri et al., 2015;
58 Huang et al., 2012). p38α is also required for the reactivation of myelin-primed T_H17 cells
59 by cDC in adoptive EAE transfer (Huang et al., 2012). A sex-dependent role of p38α in EAE
60 has been reported in myeloid cells, where pharmacological inhibition or myeloid cell
61 knockout of *p38α* ameliorated EAE clinical symptoms and inflammation in female mice
62 (Krementsov et al., 2014). The role of p38α in EAE/MS progression remains unknown.

63 Here we report that a subgroup of female mice with knockout of p38α in $CD11c^+$ cells (*KO*),
64 initially protected from EAE, develop EAE progression around 30 days post immunization
65 (dpi). We further describe clinical progression in female and male C57BL/6 wild type (*WT*)
66 mice with initially mild EAE. A reduction in $CD11c^+$ microglia and dispersed coalescent
67 parenchymal infiltration were evident at EAE progression in both conditions. In animals that
68 did not develop EAE progression, we found $CD11c^+$ microglia in association with astrocyte
69 processes and vasculature. Together, our data indicate a protective role of $CD11c^+$
70 microglia in controlling immune cell parenchymal infiltration during chronic autoimmune
71 demyelination.

72

73

74

75

76 **Materials and Methods**

77 **Animals**

78 Female and male C57BL/6 *WT* (JAX stock #000664), *p38α*$^{fl/fl}$ (*Floxed*) ([B6.129-
79 *Mapk14*<tm1.2Otsu], Riken #RBRC02192), and *p38α*$^{\Delta CD11c}$ (*KO*) mice 12 weeks old were
80 used to study EAE progression. Mice carrying the *p38α floxed* allele were crossed with mice
81 expressing Cre recombinase under the CD11c promoter ([C57BL/6J-Tg(*Itgax*-cre-
82 EGFP)4097Ach/J], JAX stock #007567). Offsprings were genotyped for the homologous
83 presence of *p38α floxed* allele and *Cre* insert as described earlier (Lo et al., 2014). Animals
84 were maintained in accordance with the NIH Guide for the Care and Use of Laboratory
85 Animals. Experimental protocols were approved by the Institutional Animal Care and Use
86 Committee at the University of California, Davis.

87 **EAE induction**

88 EAE was induced in female and male mice at the age of 12 weeks as described earlier with
89 some modifications (Chechneva et al., 2011). In brief, mice were injected subcutaneously
90 at two flank sites with an emulsion of myelin oligodendrocyte glycoprotein peptide fragment
91 that spans amino acids 35-55 (MOG) (New England Peptide) in incomplete Freund's
92 adjuvant supplemented with 500 µg Mycobacterium tuberculosis H37Ra (Difco). Our
93 previously described EAE model with MOG prepared by sonication causes severe EAE in
94 C57BL/6 mice (Chechneva et al., 2011). Sonication changes biochemical composition of
95 MOG epitopes and/or Mycobacterium tuberculosis causing an enhanced immune response
96 (Adelmann et al., 1995). In *KO* mice, sonicated MOG causes mild EAE. EAE in *KO* and
97 *Floxed* control mice was induced by MOG (300 µg) emulsion prepared by quick sonication
98 (3x5 sec on ice). To induce mild EAE in *WT* mice, MOG (150 µg) was homogenized with 2
99 syringes connected by a stopcock (twice 10 min with 3 h interval on ice). Emulsion was

100 kept in the dark at 4^0C between mixing and before preparing into individual doses in
101 syringes. All mice received 200 ng of pertussis toxin (PTX) (List Biological Labs)
102 intraperitoneally (i. p.) on day 0 and 2. The severity of clinical symptoms was evaluated
103 using following neurologic scoring for EAE: 0 - no deficit; 0.5 - mild loss of tail tone; 1 -
104 complete loss of tail tone; 1.5 - mildly impaired righting reflex; 2 - abnormal gait (ataxia)
105 and/or impaired righting reflex; 2.5- single hind limb paresis and ataxia; 3 - double hind limb
106 paresis; 3.5 - single limb paralysis and paresis of second limb / paresis of both hind limbs
107 and weakness of front limbs; 4 - full paralysis of two limbs; 4.5 - hind limb paralysis with hind
108 body paresis; 5 – moribund or death. Animals were monitored and scored daily. At 30 dpi,
109 *WT* mice were organized in three groups, according to clinical phenotype. Mild EAE was
110 defined by chronic mild clinical symptoms throughout EAE course, ranging from loss of tail
111 tone to abnormal gait/paresis (maximum score 3). Severe EAE included animals with
112 minimal recovery from EAE peak and scores of 3.5 (single limb paralysis) and above
113 throughout chronic EAE course. EAE progression was identified by transition from mild to
114 severe disease around 30 dpi with an acute increase in clinical score by 1-2.5 points.

115 **Histology and pathological scoring**

116 Histological analysis was performed as described earlier (Chechneva et al., 2011). Briefly,
117 mice were anesthetized with isoflurane and perfused with ice cold phosphate buffered saline
118 (PBS). Lumbar spinal cords were dissected, cryopreserved in 20% sucrose, embedded in
119 OCT compound and cut in 15 µm sections on the cryostat. For Luxol Fast Blue (LFB)
120 staining, sections were incubated with 0.1% LFB solution at 60^0C for 16 h followed by
121 differentiation with 0.05% lithium carbonate and co-stained with 0.1% Cresyl Violet (Nissl).
122 Slides were mounted using Cytoseal-60 medium and images were acquired on Keyence
123 BZ-9000 microscope. For pathological assessment, for each animal, six sections of the
124 lumbar spinal cord in the interval of 180 µm were scored by blinded investigator for

125 infiltration, vacuolation caused by swollen axon sheaths and demyelination. We used
126 following scoring system: 0 - absence of lesion and infiltration; 1 - not clearly visible lesions
127 and infiltration, 2 – clearly visible lesions and infiltration, 3 – prominent multifocal lesions
128 and infiltration, 4 – marked continuous lesions and infiltration (Anderson et al., 2011).

129 **Immunohistochemistry**

130 For immunostaining, sections were washed with PBS to remove residues of OCT
131 compound. Nonspecific binding of antibodies was blocked using 10% normal serum in 0.2%
132 Triton-X in PBS. Samples were incubated with rabbit anti-Iba1 (ionized calcium binding
133 adaptor molecule 1; 1:500; Wako 019-19741), rabbit anti-CD4 (1:200; Abcam ab183685),
134 rat anti-CD4 (1:100; BD Pharmingen 550280), rat anti-CD31 (1:200; Abcam ab56299),
135 chicken anti-GFP (1:500, Abcam ab13970), rabbit anti-CCL2 (1:200, Millipore AB1834P),
136 DyLight 594-Lectin (1:200, Vector Laboratories DL-1177) overnight at 4 °C. Fluorophore-
137 conjugated secondary antibodies Alexa Fluor 488, 555 or 647 (1:1000; Life Technologies)
138 were used to detect primary antibody. Slides were mounted using DAPI Fluoromount-G
139 (SouthernBiotech). Images were acquired on Nikon Eclipse 90i (A1) microscope. For DAB
140 staining, sections were treated with 1% H_2O_2 to stop endogenous peroxidase activity before
141 incubation with blocking serum. Samples were incubated with primary antibody. HRP-
142 conjugated secondary antibody was used to detect primary antibody. Positive signal was
143 visualized using ImmPACT DAB Peroxidase substrate kit (Vector labs). Slides were
144 mounted using Cytoseal-60 medium and images were acquired on Keyence BZ-9000
145 microscope. For fluorescent and DAB staining negative controls omitting primary antibody
146 were performed. Images were processed using Adobe Photoshop CC.

147 **Flow cytometry analysis**

148 Mice were deeply anesthetized and transcardially perfused with ice-cold PBS for 3 min with
149 a flow rate at 3 ml/min. All steps were performed on ice (4°C), unless otherwise stated. Brain
150 and spinal cord were dissected and placed in ice-cold HBSS (Hank's Balanced Salt
151 Solution) in 2.5 cm culture dish. For tissue digestion, papain resulted in a higher cell yield
152 compared to collagenase. However, we found that papain digestion resulted in the loss of
153 CD11c expression on the cell surface. Therefore, CNS tissue for all FACS experiments were
154 digested using collagenase. Collagenase D (Roche) 1 mg/ml and 0.02 mg/ml with 100 U/ml
155 DNAse I (Worthington) were added to each dish (final concentration), tissue was chopped
156 into ~1-2 mm^3 pieces and incubated while shaking at 100 rpm at 37 °C with 5% CO_2 for 20
157 min. Enzymatic activity was blocked by EDTA at final concentration 2 mM. Tissue was
158 homogenized in Dounce homogenizer (5-8 strokes) and cell suspension was passed
159 through a 100 µm cell strainer (Corning) in 50 ml falcon tubes. Cells were collected at 350
160 x g for 5 min at 4°C, resuspended in 37% Percoll (GE Healthcare), transferred to 15 ml
161 falcon tubes and centrifuged at 500 x g for 15 min with 0 brake at 4^0C. Cell myelin layer
162 containing cell debris was aspirated. Cell pellet was resuspended in cold 0.5 ml RBC lysis
163 buffer (Biolegend, 420301), transferred to 15 ml falcon tubes and incubated for 30 sec. 5 ml
164 PBS was added before centrifugation at 350 x g at 4^0C for 5 min. Cells were resuspended
165 in FACS buffer (PBS plus 1% BSA and 0.1% sodium azide), counted using hemocytometer
166 and transferred to staining plates (Fisher Scientific, 12565502). Following 15 min of Fc
167 receptors blocking with CD16/CD32 antibody (BD Pharmingen), cells were stained with
168 fluorophore-conjugated antibodies: CD11b BV605 (1:200, clone M1/70, Biolegend), CD45
169 PerCP-Cy5.5 (1:200, clone 30-F11, Biolegend), Ly6G APC-Cy7 (1:200, clone 1A8, BD
170 Biosciences), CD11c FITC (1:100, clone N418, Biolegend), CD11c APC (1:100, clone
171 N418, Biolegend) for 30-60 min. Cells were washed twice with FACS buffer and once with
172 PBS to remove residues of BSA, then incubated with dead cell dye, Zombie red (1:1000 in

173 PBS, Biolegend) for 15 min. After washing, cells were analyzed on Attune NxT Acoustic
174 Focusing Cytometer (Life Technologies). For cytokine detection, cells were counted and
175 incubated in RPMI-1640 medium supplemented with 10% FBS, 2 mM glutamax, 1 mM
176 sodium pyruvate, 0.1 mM NEAA, 100 U penicillin/streptomycin, 50 μM β-ME with Golgi plug
177 (BD Biosciences, 555029) for 1 h at 37^0C with 5% CO_2. Phorbol 12-myristate 13-acetate
178 (PMA, 50 ng/ml final concentration) and ionomycin (750 ng/ml final concentration) were
179 added to incubate for 4-5 h at 37^0C. Fc receptors were blocked as described above and
180 cells were stained with CD3e FITC (1:200, clone 145-2C11, BD Pharmingen) or CD3e PE-
181 Cy7 (1:200, clone 145-2C11, BD Pharmingen). Dead cells were labeled using Violet
182 fluorescence reactive dye for 20 min (1:1000, ThermoFisher, Cat# L34963). Cells were fixed
183 for 15 min using BD Cytofix/Cytoperm reagent (BD Biosciences, 554722). After washing
184 with BD Perm/Wash (BD Biosciences, 554723) twice, cells were incubated overnight at 4^0C
185 with IFN-γ APC (1:25, Clone XMG1.2, Biolegends) and IL-17 PE (1:50, Clone TC11-18H10,
186 BD Pharmingen) in Perm/Wash buffer. Cells were washed and resuspended in FACS buffer
187 for analysis on Attune NxT Acoustic Focusing Cytometer (Life Technologies). Unstained
188 cells, single stain controls and stained AbC Total Antibody Compensation beads (Thermo
189 Fisher, A10497) were used for each experiment to determine compensation parameters.
190 For isotype control of fluorescence minus one, antibody was substituted by fluorophore-
191 conjugated isotype control. Acquired data were analyzed using FlowJo software (TreeStar).
192 To define populations of $CD11c^+$ microglia, we found gating on $CD11b^+$ and $CD45^+$ cells
193 from the pool of $CD11c^+$ cells was more accurate than gating of $CD11c^+$ cells from
194 $CD11b^+CD45^{low}$ due to the lack of clear separation of macrophages/monocytes from
195 microglia within $CD11b^+CD45^{int}$ population. Absolute numbers of cell types isolated from the
196 CNS was determined by multiplying the total number of live cells to the proportion of the cell
197 type acquired by flow cytometer. Quantitative data were presented in absolute numbers.

198 **Proliferation assay of CD11c$^+$ cells**

199 EdU is a thymidine nucleoside analog that incorporates into DNA during S-phase of the cell
200 cycle. To label proliferating cells, animals were pulsed twice with 12 mg/kg EdU
201 intraperitoneal injection in 12 h interval. 24 h after the first injection, animals were deeply
202 anesthetized and perfused with ice-cold PBS. Brain and spinal cord were dissected, and
203 cells were isolated as described above. Following steps were performed on ice (4°C), unless
204 otherwise stated. Fc receptors were blocked with CD16/CD32 antibody (BD Pharmingen)
205 for 15 min and cells were stained with fluorophore-conjugated antibodies: CD11b BV605
206 (1:200, clone M1/70, Biolegend), CD45 PerCP-Cy5.5 (1:200, clone 30-F11, Biolegend) and
207 CD11c APC (1:100, clone N418, Biolegend) for 30 min. Zombie violet (1:1000, Biolegend)
208 was used to label dead cells. Cells were then fixed with 4% PFA for 15 min at RT. After
209 washing with 1% BSA in PBS, cells were permeabilized with saponin-based
210 permeabilization and wash reagent (Invitrogen, Click-iT Plus EdU Kit) for 15 min at RT.
211 Residues of permeabilization buffer were removed by centrifugation at 350 x g for 5 min.
212 EdU was detected by incubation with freshly prepared Click-iT cocktail containing Tris-HCl
213 (100 mM, pH 7.6), 2 mM $CuSO_4$, 2.5 µM Sulfo-Cy3 Azide (Limiprobe) and 100 mM ascorbic
214 acid for 15 min at RT in the dark. Cells were washed with FACS buffer and analyzed on
215 Attune NxT Acoustic Focusing Cytometer (Life Technologies). For Cy3 single stain
216 compensation control we used cells isolated from bone marrow. Proliferation rate was
217 determined as the percentage of EdU$^+$ cells within cell populations.

218 **p38 kinase activity**

219 p38 MAPK activity was assessed by quantifying phospho-p38 MAPK expression levels. *KO*
220 and *Floxed* female and male mice were intraperitoneally injected with 3 mg/kg LPS
221 (O111:B4, Sigma). 24 h after, mice were deeply anesthetized and spleens were isolated,
222 chopped in ice-cold HBSS, and enzymatically digested for 20 min at 37^{0}C. Digested tissue

223 was passed through a 70 µm cell strainer into 50 ml falcon tubes using the backside of 1 ml
224 syringe. Cells were pelleted by centrifugation at 350 x g at 4^0C for 5 min and resuspended
225 in ice-cold 1 ml RBC lysis buffer. After washing and centrifugation, cells were resuspended
226 in MACS buffer (PBS with 0.5% BSA and 2 mM EDTA) and counted using
227 hematocytometer. After centrifugation, cells were resuspended and incubated in MACS
228 buffer containing Fc blocker and CD11c MicroBeads (Miltenyi Biotec) according to
229 manufacturer instruction. $CD11c^+$ cells were isolated using LS columns (Miltenyi Biotec,
230 Cat# 130-108-338), pelleted and processed for staining on ice (4°C). After Fc receptor
231 blocking with CD16/CD32 antibody (BD Pharmingen), cells were incubated with
232 fluorophore-conjugated antibodies CD11b BV605 (1:200, clone M1/70, Biolegend) and
233 CD11c APC (1:100, clone N418, Biolegend) for 30-60 min. After washing, cells were
234 incubated with dead cell dye Zombie red (1:1000 in PBS, Biolegend) for 15 min. Cells were
235 fixed for 15 min using BD Cytofix/Cytoperm reagent. After washing with BD Perm/Wash,
236 cells were incubated overnight with phospho-p38 MAPK PE (Thr180/Tyr182 (3D7), 1:50,
237 Cell Signaling). Cells were analyzed on Attune NxT Acoustic Focusing Cytometer (Life
238 Technologies). Unstained cells, single stain controls, stained AbC Total Antibody
239 Compensation beads and isotype controls were used for each experiment. Acquired data
240 were analyzed using FlowJo software (TreeStar).

241 **RNA isolation and qPCR**

242 RNA transcription levels of CCL2 in the lumbar spinal cord was analyzed using qPCR as
243 described earlier (Chechneva et al., 2011). Briefly, mice were anesthetized and
244 transcardially perfused with ice-cold PBS. Lumbar spinal cords were dissected and stored
245 separately in liquid nitrogen. Total RNA was isolated from spinal cord tissue using Direct-
246 zol RNA MiniPrep Kit (Zymo Research) following the manufacturer protocol. RNA at purity
247 $OD_{260/280}$ ratio between 1.8 and 2.0 was reverse-transcribed to cDNA using Multiscribe

248 reverse transcriptase (Applied Biosystems). TaqMan gene expression assay (Applied
249 Biosystems) was used for *CCL2* (Mm00441242_m1). All experimental samples were
250 normalized to the expression level of *GAPDH* (4352339E Applied Biosystems). Relative
251 quantification of fold-change was performed by applying the $2^{-\Delta\Delta}$CT method and comparing
252 Cp values of individual mice (Livak and Schmittgen, 2001).

253 **Statistics**

254 Statistical analysis was performed using GraphPad Prism 7.5. The numbers of animals per
255 group used for each study are shown in the figures as individual dots or indicated in the
256 figure legend. EAE clinical scores were pooled from four independent EAE experiments and
257 evaluated for statistical significance using Two-way ANOVA with Sidak's multiple
258 comparisons test. One-way ANOVA with Tukey's post hoc test was used to analyze data in
259 Table 1. Two group experiments were analyzed using Student's t-test. Experiments with
260 three and more groups were analyzed using One-way ANOVA with Tukey's post hoc test.
261 In all figures, data are represented as mean ± s.e.m. In all cases, probability values less
262 than 0.05 were considered statistically significant. Images were assembled using Adobe
263 Illustrator CC.

264 **Results**

265 **Female mice with knockout of *p38α* in CD11c$^+$ cells are susceptible to EAE**
266 **progression**

267 We induced EAE in *KO* and *Floxed* female and male mice and followed EAE clinical
268 symptoms for 60 days. As reported earlier, *Floxed* mice developed chronic severe disease,
269 while *KO* mice were protected and initially displayed mild EAE (Huang et al., 2012;
270 Krementsov et al., 2014) (Fig. 1A, Table 1). EAE onset and peak were delayed in *KO*
271 females compared to *KO* males (Fig. 1A, Table 1). At 30 dpi, 58% of *KO* females underwent

272 clinical progression and transition from mild to severe disease with a sudden increase in
273 clinical score by 1-2.5 points (Fig. 1A, Table 1). No progression of EAE clinical symptoms
274 was observed in *KO* males.
275 We analyzed EAE pathology at 30 dpi in the lumbar spinal cord of *KO* and *Floxed* mice. In
276 progressed *KO* females, we found dispersed parenchymal infiltration, demyelination, and
277 $CD4^+$ T cells and $Iba1^+$ macrophages/reactive microglia densely scattered throughout the
278 white matter parenchyma (Fig. 1B-D). In contrast, in *KO* males we found a distinct pattern
279 of immune cell infiltration where peripheral immune cells clustered at perivascular areas and
280 the meninges, and $CD4^+$ T cells had rare appearance in the parenchyma (Fig. 1B-D). T cells
281 that invaded CNS parenchyma in progressed *KO* females were enriched in INF-γ^+ T_H1
282 population (Supplementary Fig. 1A-D). We found an increase in transcription level of *IL-12b*
283 (also known as *IL-12p40*), a driver of T_H1 cell differentiation (Balashov et al., 1997)
284 (Supplementary Fig. 1E). In *KO* females with mild EAE that did not transition to EAE
285 progression we observed minor immune cell infiltration (Fig. 1B-D). In *Floxed* mice
286 sustained parenchymal infiltration and demyelination corresponding to chronic severe
287 disease state were evident (Fig. 1B-D).
288 We further analyzed CNS infiltrates using flow cytometry. $CD45^+$ cells were significantly
289 increased in the brain and spinal cord of progressed *KO* females compared to *KO* males
290 and mild non-progressed *KO* females (Fig. 1E, 1H). $CD45^+$ cells included $Ly6G^+$ neutrophils
291 (Fig. 1F, 1I) and $CD11b^+CD45^{hi}$ macrophages/monocytes (Fig. 1G, 1J). *KO* females without
292 progression had low numbers of infiltrating immune cells (Fig. 1E-J). There were no
293 significant differences in the numbers of $CD11b^+CD45^{lo}$ microglia between groups (Fig. 1G,
294 1K). We conclude that peripheral immune cell infiltration contributes to EAE progression in
295 *KO* female mice.

296

297 **Reduction in CD11c$^+$ microglia in *KO* female mice**

298 CD11c$^+$ cells play an active role in the pathogenesis of MS and EAE (Di Mitri et al., 2015;
299 Giles et al., 2018; Huang et al., 2012; Krementsov et al., 2014; Merad et al., 2013; Mundt
300 et al., 2019). Using flow cytometry, we found an increase in CD11c$^+$ cells driven by an
301 increase in the CD11c$^+$CD11b$^+$CD45^{hi} moDC in the brain and spinal cord of progressed *KO*
302 females (Fig. 2A-D). An increase in the number of CD11c$^+$CD11b$^-$CD45^{hi} cDC was found in
303 progressed compared to non-progressed *KO* females with mild EAE, reflecting the disease
304 pathology (Fig. 2E). Surprisingly, a significant reduction in CD11c$^+$CD11b$^+$CD45^{lo} or CD11c$^+$
305 microglia was found in progressed and non-progressed *KO* females (Fig. 2C, F). Gating on
306 CD11c$^+$ microglia from the pool of CD11b$^+$CD45^{lo} cells resulted in a similar outcome
307 (Supplementary Fig. 2A-B).

308 In EAE, microglia increase in numbers by proliferation (Ajami et al., 2011; Jordao et al.,
309 2019). To test whether proliferation of CD11c$^+$ microglia is dependent on p38 signaling we
310 compared cell proliferation in MOG-PTX immunized *Floxed* and *KO* mice that did not
311 develop clinical symptoms by 30 dpi. Under this condition, we found an increase in numbers
312 of CNS associated CD45$^+$ immune cells, indicating a primed immune response
313 (Supplementary Fig. 3A). The numbers and proliferation rates of CNS associated cDC or
314 moDC were not affected by knockout of *p38α* (Fig. 2G-K). However, we found that numbers
315 and proliferation rate of CD11c$^+$ microglia were decreased in *KO* female compared to *KO*
316 male mice (Fig. 2G, 2L-M). Proliferation rate of macrophages/monocytes or total microglia
317 were not different between groups (Supplementary Fig. 3B-D). To demonstrate efficiency
318 of *p38α* knockout, expression of the activated form of p38 MAPK, phospho-p38 MAPK (p-
319 p38), was examined in splenocytes after LPS stimulation. Reduced expression of p-p38
320 was found in CD11c$^+$ splenocytes in *KO* female and *KO* male mice compared to *Floxed*

321 control (Supplementary Fig. 3E-F). We conclude that EAE progression in *KO* female mice
322 is associated with p38α-dependent reduction in CD11c$^+$ microglia.

323 **Reduction in CD11c$^+$ microglia occurs at EAE progression in *WT* mice**

324 To study EAE progression in *WT* mice, we induced EAE in C57BL/6 mice with MOG
325 prepared by syringe emulsification. This EAE model resulted in three distinct EAE
326 phenotypes: mild (42%), severe (31%) and initially mild with progression around 30 dpi
327 (27%) (Fig. 3A, Table 2). We compared the pathology between different EAE phenotypes
328 at 30 dpi and EAE peak. Histological analysis revealed dispersed coalescent infiltration of
329 the spinal cord white matter at EAE progression compared to focal infiltrates found at EAE
330 peak (Fig. 3B). A diffuse scattering of immune cells in the parenchyma with lower density
331 than at EAE progression was observed in chronic severe EAE (Fig. 3B). In all EAE groups
332 the vast majority of parenchymal immune cells were Iba1$^+$ macrophages/reactive microglia
333 (Fig. 3C). EAE progression was associated with an increase in T_H1 and T_H17 cells
334 compared to mild and severe EAE (Supplementary Fig. 4A-D). Flow cytometry showed a
335 significant increase in CD45$^+$ cells including neutrophils, macrophages/monocytes, cDC and
336 moDC at EAE peak compared to all chronic EAE groups (Fig. 4A-K). Increase in neutrophils,
337 macrophages/monocytes, cDC and moDC was evident at EAE progression compared to
338 mild and severe EAE (Fig. 4A-K). The numbers of CD11b$^+$CD45^{lo} microglia were
339 consistently increased in all EAE groups compared to healthy control (Fig. 4C, 4L). Notable,
340 EAE progression was associated with a significant reduction in CD11c$^+$ microglia (Fig. 4E,
341 4M, Supplementary Fig. 4E-F). There were no sex-dependent differences within immune
342 cell populations between experimental conditions in *WT* mice. We conclude that clinical
343 progression during chronic EAE is associated with dispersed parenchymal infiltration and
344 involves reduction in CD11c$^+$ microglia.

345

346 **CD11c$^+$ microglia contact astrocyte processes and glia limitans**

347 Astrocytes orchestrate immune cell parenchymal infiltration (Horng et al., 2017; Kim et al.,
348 2014). We examined localization of CD11c$^+$ microglia in relation to astrocytes. Commercially
349 available antibodies were not able to detect CD11c$^+$ cells by immunohistochemistry, likely
350 due to low expression of CD11c in migrating and activated CD11c$^+$ cells (Merad et al., 2013;
351 Prodinger et al., 2011). To visualize CD11c$^+$ cells, we used expression of eGFP under the
352 CD11c promoter. In protected *KO* males, we found dendritic-like CD11c$^+$ microglia in the
353 vicinity to astrocytes and blood vessels (Fig. 5A-B). CD11c$^+$ microglia were abundant in *WT*
354 mice with chronic mild EAE (Fig. 5C). Dendritic-like CD11c$^+$ microglia with stellate thick
355 processes formed contacts with astrocytes (Fig. 5D). In progressed *KO* females,
356 disorganized processes of hypertrophic astrocytes were surrounded by infiltrating moDC /
357 ameboid CD11c$^+$ microglia (Fig. 5E-F). Dendritic-like CD11c$^+$ microglia could not be
358 differentiated from infiltrating moDC by morphology. Infiltration of immune cells into the CNS
359 parenchyma is dependent on astrocyte-derived CCL2 (Dogan et al., 2008; Kim et al., 2014;
360 Moreno et al., 2014). We found upregulation of CCL2 expression in hypertrophic reactive
361 astrocytes in progressed *KO* females (Fig. 5G-H). Our data suggest that CD11c$^+$ microglia
362 interaction with astrocytes at the glia limitans is dysregulated in EAE progression.

363 **Discussion**

364 EAE allows to study a variety of clinical features of MS (Constantinescu et al., 2011). Here
365 we demonstrate that mice that develop mild EAE after MOG immunization are primed to
366 undergo spontaneous EAE progression around 30 dpi. EAE progression appeared in 58%
367 of female mice lacking *p38α* in CD11c$^+$ cells and ~40% of *WT* mice both of which initially
368 developed mild EAE. Similar progression of clinical symptoms around 30 dpi was reported
369 in non-obese diabetic mice used as a model of EAE progression (Baker et al., 2019; Basso
370 et al., 2008; Buonvicino et al., 2019; Encinas et al., 1999; Tanabe et al., 2019). Why EAE

371 progression follows a 30 dpi pattern and what triggers progression in a fraction of animals
372 with mild EAE remains to be investigated.

373 Secondary antigenic epitope spreading has been identified as a molecular trigger in MS
374 relapse and progression involving Th1 and Th17 cells (Babaloo et al., 2015; Balashov et
375 al., 1997; McRae et al., 1995; Romme Christensen et al., 2013). Activation of epitope-
376 specific Th cells is dependent on antigen-presenting CD11c$^+$ cells (Chastain et al., 2011;
377 Giles et al., 2018; Greter et al., 2005; Mundt et al., 2019) and requires p38α for induction of
378 the Th17 population (Di Mitri et al., 2015; Huang et al., 2012). We found that both, Th1 and
379 Th17 cells were involved in chronic EAE progression in *WT* mice. However, re-activation
380 of Th1 cells through p38α-independent mechanism was enough to trigger EAE progression
381 in *KO* female mice, suggesting mechanistic differences in immune response between initial
382 EAE peak and progression of chronic EAE. *KO* males were protected from EAE
383 progression. Whether Th17 cells are required for EAE progression in males remains to be
384 examined.

385 Comparing compositions of immune cells and patterns of parenchymal infiltration between
386 EAE phenotypes, we found selective reduction in CD11c$^+$ microglia and dispersed
387 coalescent parenchymal infiltration as characteristic features of chronic EAE progression.
388 Importantly, dispersed infiltration but with lesser cell density was also evident in chronic
389 severe EAE, suggesting that dispersed, in contrast to focal infiltration is a pathological
390 hallmark of irreversible disability.

391 Signaling via p38 MAPK is involved in hormone-dependent sexual dimorphism of the
392 immune response with variable outcomes depending on cell type and condition. In
393 microglia, p38 MAPK was identified as a cause of neuropathic and inflammatory pain in
394 males in chronic constriction injury and mechanical allodynia (Sorge et al., 2015; Taves et

395 al., 2016). Testosterone-dependent increase in p38 MAPK phosphorylation in splenic and
396 peritoneal macrophages was reported in male mice after trauma-hemorrhage (Angele et al.,
397 2003). We found that p38α was involved in maintaining CD11c$^+$ microglia in female mice
398 and reduction in CD11c$^+$ microglia correlated with increased rate of EAE progression in *KO*
399 females. In contrast, protection from EAE progression in *KO* males was associated with the
400 presence of CD11c$^+$ microglia in close contact with astrocytes and at the glia limitans. A
401 biased role of p38α in driving CD11c$^+$ microglia reduction in males would explain the lack of
402 EAE progression in *KO* male mice. Defining the molecular mechanism of CD11c$^+$ microglia
403 reduction is needed to further understand the sex-specific role of p38α at EAE progression.

404 In our study, *KO* female mice showed a delay in EAE onset and peak, indicating a delay in
405 the peripheral immune response involving cDC and/or moDC. This is supported by an earlier
406 study where female mice lacking p38α in myeloid cells showed improvement of EAE clinical
407 symptoms while their male cohorts developed exacerbated EAE (Krementsov et al., 2014).
408 Reduced peripheral immune response may explain the lack of EAE progression in the
409 fraction of *KO* females with minor spinal cord infiltration. Changes in the peripheral immune
410 response within *KO* females may be caused by unequal efficiency of *p38α* deletion or
411 compensatory activity of alternative p38 MAPK subunits, such as p38β and p38δ (Huang et
412 al., 2012). Taking together, variable effects of p38α function may explain why many of p38
413 MAPK inhibitors failed to fulfill their expectations in clinical trials to date and emphasize the
414 need of cell-specific therapeutic approaches (Goldstein et al., 2010; Krementsov et al.,
415 2013).

416 Dendritic-like CD11c$^+$ microglia localized at the glia limitans are found in the brain, spinal
417 cord and optic nerve under healthy conditions and are suggested to play a role in astrocyte
418 glia limitans organization (Prodinger et al., 2011). Glia limitans astrocytic endfeet surround
419 blood-brain barrier endothelial cells and form a physical border between perivascular

420 spaces and CNS parenchyma (Horng et al., 2017). Dendritic-like CD11c$^+$ microglia were
421 abundant in the spinal cord of mice with chronic mild EAE, where immune cells were
422 restricted from entering parenchyma. These CD11c$^+$ microglia formed physical contacts
423 with astrocyte processes suggesting their direct interaction with astrocytes to limit immune
424 cell parenchymal entry. Expression of triggering receptor expressed on myeloid cells
425 (TREM2) has been associated with CD11c$^+$ microglia in EAE and an animal model of
426 Alzheimer's disease (Keren-Shaul et al., 2017; Piccio et al., 2007). Supporting the concept
427 of a potential protective role of CD11c$^+$ microglia in CNS infiltration, diffuse parenchymal
428 infiltration and increase of clinical disability in EAE was found after blockade of TREM2
429 activity with specific antibody (Piccio et al., 2007).

430 **Conclusion**

431 Our study provides novel insight into the cellular mechanisms underlying clinical
432 progression during chronic EAE. We identified reduction in CD11c$^+$ microglia and the
433 specific pattern of dispersed parenchymal infiltration as pathological hallmarks of EAE
434 progression. Our data suggest a protective role of dendritic-like CD11c$^+$ microglia in
435 controlling CNS infiltration and EAE progression through interaction with astrocytes.

436

437

Acknowledgements: This work was in parts supported by grants from National Institutes of Health (R01HD087566 to W.D.) and Shriners Hospital for Children (87310-NCA-19 to O.C.).

Author contributions

O.V.C. and F.M. designed the research, performed experiments, interpreted the data, wrote and edited the manuscript. Z.D., A.Z., D.J.D., and A.M.H. performed experiments. P.B., D.P., A.S., and W.D. interpreted the data and edited the manuscript.

Conflict of interest: The authors have declared that no conflict of interest exists.

References

Adelmann, M., et al., 1995. The N-terminal domain of the myelin oligodendrocyte glycoprotein (MOG) induces acute demyelinating experimental autoimmune encephalomyelitis in the Lewis rat. J Neuroimmunol. 63, 17-27.

Ajami, B., et al., 2011. Infiltrating monocytes trigger EAE progression, but do not contribute to the resident microglia pool. Nat Neurosci. 14, 1142-9.

Anderson, P. J., et al., 2011. Attention problems in a representative sample of extremely preterm/extremely low birth weight children. Dev Neuropsychol. 36, 57-73.

Angele, M. K., et al., 2003. Sex-specific p38 MAP kinase activation following trauma-hemorrhage: involvement of testosterone and estradiol. Am J Physiol Endocrinol Metab. 285, E189-96.

Babaloo, Z., et al., 2015. The role of Th17 cells in patients with relapsing-remitting multiple sclerosis: interleukin-17A and interleukin-17F serum levels. Immunol Lett. 164, 76-80.

Baecher-Allan, C., et al., 2018. Multiple Sclerosis: Mechanisms and Immunotherapy. Neuron. 97, 742-768.

Baker, D., et al., 2019. Autoimmune encephalomyelitis in NOD mice is not initially a progressive multiple sclerosis model. Ann Clin Transl Neurol. 6, 1362-1372.

Balashov, K. E., et al., 1997. Increased interleukin 12 production in progressive multiple sclerosis: induction by activated CD4+ T cells via CD40 ligand. Proc Natl Acad Sci U S A. 94, 599-603.

Basso, A. S., et al., 2008. Reversal of axonal loss and disability in a mouse model of progressive multiple sclerosis. J Clin Invest. 118, 1532-43.

Buonvicino, D., et al., 2019. Neuroimmunological characterization of a mouse model of primary progressive experimental autoimmune encephalomyelitis and effects of immunosuppressive or neuroprotective strategies on disease evolution. Exp Neurol. 322, 113065.

Butovsky, O., et al., 2006. Glatiramer acetate fights against Alzheimer's disease by inducing dendritic-like microglia expressing insulin-like growth factor 1. Proc Natl Acad Sci U S A. 103, 11784-9.

Chastain, E. M., et al., 2011. The role of antigen presenting cells in multiple sclerosis. Biochim Biophys Acta. 1812, 265-74.

Chechneva, O. V., et al., 2011. Low dose dextromethorphan attenuates moderate experimental autoimmune encephalomyelitis by inhibiting NOX2 and reducing peripheral immune cells infiltration in the spinal cord. Neurobiol Dis. 44, 63-72.

Constantinescu, C. S., et al., 2011. Experimental autoimmune encephalomyelitis (EAE) as a model for multiple sclerosis (MS). Br J Pharmacol. 164, 1079-106.

Coret, F., et al., 2018. Onset of secondary progressive multiple sclerosis is not influenced by current relapsing multiple sclerosis therapies. Mult Scler J Exp Transl Clin. 4, 2055217318783347.

Di Mitri, D., et al., 2015. The p38 mitogen-activated protein kinase cascade modulates T helper type 17 differentiation and functionality in multiple sclerosis. Immunology. 146, 251-63.

Dogan, R. N., et al., 2008. Production of CCL2 by central nervous system cells regulates development of murine experimental autoimmune encephalomyelitis through the recruitment of TNF- and iNOS-expressing macrophages and myeloid dendritic cells. J Immunol. 180, 7376-84.

Encinas, J. A., et al., 1999. QTL influencing autoimmune diabetes and encephalomyelitis map to a 0.15-cM region containing Il2. Nat Genet. 21, 158-60.

Fischer, H. G., Reichmann, G., 2001. Brain dendritic cells and macrophages/microglia in central nervous system inflammation. J Immunol. 166, 2717-26.

Ford, A. L., et al., 1995. Normal adult ramified microglia separated from other central nervous system macrophages by flow cytometric sorting. Phenotypic differences defined and direct ex vivo antigen presentation to myelin basic protein-reactive CD4+ T cells compared. J Immunol. 154, 4309-21.

Giles, D. A., et al., 2018. CNS-resident classical DCs play a critical role in CNS autoimmune disease. J Clin Invest. 128, 5322-5334.

Goldschmidt, C., McGinley, M. P., 2021. Advances in the Treatment of Multiple Sclerosis. Neurol Clin. 39, 21-33.

499 Goldstein, D. M., et al., 2010. Selective p38alpha inhibitors clinically evaluated for the treatment of
500 chronic inflammatory disorders. J Med Chem. 53, 2345-53.
501 Greter, M., et al., 2005. Dendritic cells permit immune invasion of the CNS in an animal model of
502 multiple sclerosis. Nat Med. 11, 328-34.
503 Hagemeyer, N., et al., 2017. Microglia contribute to normal myelinogenesis and to oligodendrocyte
504 progenitor maintenance during adulthood. Acta Neuropathol. 134, 441-458.
505 Horng, S., et al., 2017. Astrocytic tight junctions control inflammatory CNS lesion pathogenesis. J
506 Clin Invest. 127, 3136-3151.
507 Huang, G., et al., 2012. Signaling via the kinase p38alpha programs dendritic cells to drive TH17
508 differentiation and autoimmune inflammation. Nat Immunol. 13, 152-61.
509 Jordao, M. J. C., et al., 2019. Single-cell profiling identifies myeloid cell subsets with distinct fates
510 during neuroinflammation. Science. 363.
511 Kamphuis, W., et al., 2016. Transcriptional profiling of CD11c-positive microglia accumulating
512 around amyloid plaques in a mouse model for Alzheimer's disease. Biochim Biophys Acta.
513 1862, 1847-60.
514 Keren-Shaul, H., et al., 2017. A Unique Microglia Type Associated with Restricting Development of
515 Alzheimer's Disease. Cell. 169, 1276-1290 e17.
516 Kim, R. Y., et al., 2014. Astrocyte CCL2 sustains immune cell infiltration in chronic experimental
517 autoimmune encephalomyelitis. J Neuroimmunol. 274, 53-61.
518 Krementsov, D. N., et al., 2014. Sex-specific control of central nervous system autoimmunity by p38
519 mitogen-activated protein kinase signaling in myeloid cells. Ann Neurol. 75, 50-66.
520 Krementsov, D. N., et al., 2013. The emerging role of p38 mitogen-activated protein kinase in
521 multiple sclerosis and its models. Mol Cell Biol. 33, 3728-34.
522 Livak, K. J., Schmittgen, T. D., 2001. Analysis of relative gene expression data using real-time
523 quantitative PCR and the 2(-Delta Delta C(T)) Method. Methods. 25, 402-8.
524 Lo, U., et al., 2014. p38alpha (MAPK14) critically regulates the immunological response and the
525 production of specific cytokines and chemokines in astrocytes. Sci Rep. 4, 7405.
526 Lock, C., et al., 2002. Gene-microarray analysis of multiple sclerosis lesions yields new targets
527 validated in autoimmune encephalomyelitis. Nat Med. 8, 500-8.
528 McRae, B. L., et al., 1995. Functional evidence for epitope spreading in the relapsing pathology of
529 experimental autoimmune encephalomyelitis. J Exp Med. 182, 75-85.
530 Merad, M., et al., 2013. The dendritic cell lineage: ontogeny and function of dendritic cells and their
531 subsets in the steady state and the inflamed setting. Annu Rev Immunol. 31, 563-604.
532 Miller, S. D., et al., 2007. Antigen presentation in the CNS by myeloid dendritic cells drives
533 progression of relapsing experimental autoimmune encephalomyelitis. Ann N Y Acad Sci.
534 1103, 179-91.
535 Moreno, M., et al., 2014. Conditional ablation of astroglial CCL2 suppresses CNS accumulation of
536 M1 macrophages and preserves axons in mice with MOG peptide EAE. J Neurosci. 34,
537 8175-85.
538 Mundt, S., et al., 2019. Conventional DCs sample and present myelin antigens in the healthy CNS
539 and allow parenchymal T cell entry to initiate neuroinflammation. Sci Immunol. 4.
540 Piccio, L., et al., 2007. Blockade of TREM-2 exacerbates experimental autoimmune
541 encephalomyelitis. Eur J Immunol. 37, 1290-301.
542 Prodinger, C., et al., 2011. CD11c-expressing cells reside in the juxtavascular parenchyma and
543 extend processes into the glia limitans of the mouse nervous system. Acta Neuropathol. 121,
544 445-58.
545 Romme Christensen, J., et al., 2013. Systemic inflammation in progressive multiple sclerosis
546 involves follicular T-helper, Th17- and activated B-cells and correlates with progression.
547 PLoS One. 8, e57820.
548 Sato-Hashimoto, M., et al., 2019. Microglial SIRPalpha regulates the emergence of CD11c(+)
549 microglia and demyelination damage in white matter. Elife. 8.
550 Serafini, B., et al., 2000. Intracerebral recruitment and maturation of dendritic cells in the onset and
551 progression of experimental autoimmune encephalomyelitis. Am J Pathol. 157, 1991-2002.
552 Sorge, R. E., et al., 2015. Different immune cells mediate mechanical pain hypersensitivity in male
553 and female mice. Nat Neurosci. 18, 1081-3.

554 Tanabe, S., et al., 2019. Microglia suppress the secondary progression of autoimmune
555 encephalomyelitis. Glia. 67, 1694-1704.
556 Taves, S., et al., 2016. Spinal inhibition of p38 MAP kinase reduces inflammatory and neuropathic
557 pain in male but not female mice: Sex-dependent microglial signaling in the spinal cord. Brain
558 Behav Immun. 55, 70-81.
559 Wlodarczyk, A., et al., 2018. CSF1R Stimulation Promotes Increased Neuroprotection by CD11c+
560 Microglia in EAE. Front Cell Neurosci. 12, 523.
561 Wlodarczyk, A., et al., 2015. Pathologic and Protective Roles for Microglial Subsets and Bone
562 Marrow- and Blood-Derived Myeloid Cells in Central Nervous System Inflammation. Front
563 Immunol. 6, 463.
564 Wlodarczyk, A., et al., 2017. A novel microglial subset plays a key role in myelinogenesis in
565 developing brain. EMBO J. 36, 3292-3308.
566 Zarubin, T., Han, J., 2005. Activation and signaling of the p38 MAP kinase pathway. Cell Res. 15,
567 11-8.
568 Zhang, T., et al., 2015. Beta-interferon exposure and onset of secondary progressive multiple
569 sclerosis. Eur J Neurol. 22, 990-1000.

570

571

572 **Table 1. Clinical assessment of EAE in *p38α Floxed* and CD11c promoter-driven**
573 ***p38α KO* female and male mice**

Group	n	Onset	Mean score 1st peak	Mean score d26	Mean score d32	Max severity from d29	Duration of paralysis d29 – d60	Score at d60	Survival by d60
Floxed males	41	11.2 ± 0.2	4.2 ± 0.1	3.2 ± 0.2	3.4 ± 0.2	3.9 ± 0.1	25.9 ± 1.8	3.7 ± 0.2	90.2%
Floxed females	32	12.4 ± 0.4	4.0 ± 0.1	3.2 ± 0.2	3.3 ± 0.2	3.7 ± 0.2	23.9 ± 2.3	3.4 ± 0.2	90.6%
KO males	47	12.2 ± 0.3	3.3 ± 0.1***	2.2 ± 0.2***	2.1 ± 0.2***	2.7 ± 0.2***	10.0 ± 2.1***	2.1 ± 0.2***	95.7%
KO females Mild	17	13.2 ± 0.4*	2.9 ± 0.2***	2.0 ± 0.2***	2.1 ± 0.1**	2.3 ± 0.1***	0 ***	2.0 ± 0.2***	100%
KO females Prog	23	14.6 ± 0.8###	3.6 ± 0.2$	2.6 ± 0.3	3.5 ± 0.2###	4.1 ± 0.1###	19.4 ± 2.5#	3.7 ± 0.2###	91.3%

574 Data are the mean ± s.e.m. **P*<0.05, ***P*<0.01, ****P*<0.001, comparing between same
575 sex *Floxed* and *KO* mice. #*P*<0.05, ###*P*<0.001, comparing between females and males of
576 the same genotype. $*P*<0.05, comparing between *KO* females with and without
577 progression. *P* values were determined by One-way ANOVA with Tukey's post hoc test.
578 d, day after immunization; Prog, progression.

579

580 **Table 2. Clinical assessment of EAE in C57BL/6 *WT* mice**

Group	n	Onset	Mean score 1st peak	Mean score d26	Mean score d32	Max severity from d29	Duration of paralysis d29 – d40	Score at d40	Survival by d40
Mild males	14	11.3 ± 0.2	3.7 ± 0.1	2.5 ± 0.1	2.5 ± 0.2	2.9 ± 0.1	0.6 ± 1.3	2.6 ± 0.1	100%
Mild females	9	12.0 ± 0.5	3.3 ± 0.2	2.3 ± 0.1	2.4 ± 0.2	2.7 ± 0.2	1.3 ± 0.9	2.6 ± 0.2	100%
Severe males	9	11.9 ± 0.5	3.9 ± 0.1	3.5 ± 0.1***	3.4 ± 0.1**	3.7 ± 0.1***	7.9 ± 1.4***	3.4 ± 0.1***	100%
Severe females	8	11.9 ± 0.3	4.1 ± 0.1*	3.8 ± 0.1***	3.5 ± 0.2**	3.9 ± 0.1***	10.4 ± 0.7	3.9 ± 0.1***	87.5%
Prog males	10	13.3 ± 0.8*	3.7 ± 0.2	2.6 ± 0.1###	3.5 ± 0.2***	4.1 ± 0.1***	9.5 ± 1.3***	3.9 ± 0.1***	100%
Prog females	5	12.6 ± 0.7	3.6 ± 0.2	2.4 ± 0.2###	3.1 ± 0.2	3.8 ± 0.1***	6.6 ± 1.6*	3.8 ± 0.1***	100%

581 Data are the mean ± s.e.m. *P<0.05, **P<0.01, ***P<0.001, comparing to same sex Mild
582 EAE. #P<0.05, ##P<0.01, ###P<0.001 comparing to same sex Severe EAE. P values were
583 determined by One-way ANOVA with Tukey's post hoc test. d, day after immunization;
584 Prog, progression.

585

586

587

588 **Figures**

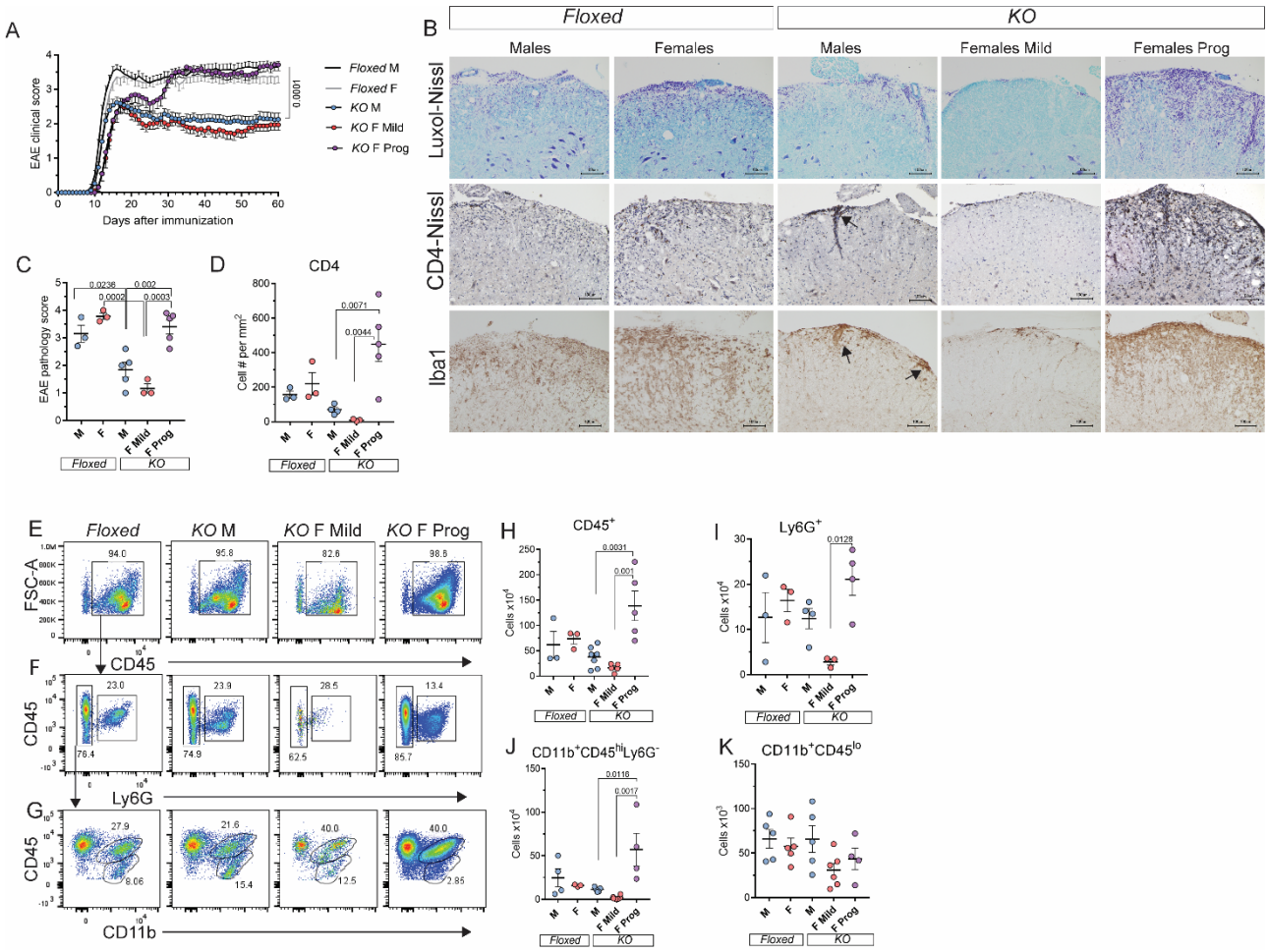

589

590 **Fig. 1. Female mice with knockout of *p38α* in CD11c⁺ cells are susceptible to EAE**
591 **progression with dispersed parenchymal infiltration.**
592 (A) *p38α Floxed* control and CD11c promoter-driven *KO* female and male mice were
593 immunized with MOG prepared by sonication. EAE clinical scores were monitored daily for
594 60 dpi. Data are representative of four independent experiments with n = 41 for *Floxed*
595 males, n = 32 for *Floxed* females, n = 47 for *KO* males, n = 23 for *KO* females with
596 progression, and n = 17 for *KO* females with chronic mild EAE. *P* values were determined
597 by two-way ANOVA with Sidak's multiple comparisons test. (B) Representative images of
598 Luxol-Nissl staining, $CD4^+$ T cells and $Iba1^+$ macrophages/microglia in the lumbar spinal
599 cord at 30 dpi. Clusters of immune cells at the meninges and perivascular areas in *KO* males
600 (arrows). Scale bar 100 µm. (C) Pathological scoring of chronic EAE based on the severity
601 of infiltration and demyelination. Data are representative of two independent experiments.
602 (D) Quantification of $CD4^+$ T cells in the white matter parenchyma. (E-G) Flow cytometry
603 analysis of $CD45^+$ cells, $Ly6G^+$ neutrophils, $CD11b^+CD45^{hi}$ macrophages/monocytes and
604 $CD11b^+CD45^{lo}$ microglia isolated from the brain and spinal cord at 30 dpi. (H-K)
605 Quantification of $CD45^+$ cells, $Ly6G^+$ neutrophils, $CD11b^+CD45^{hi}$ macrophages/monocytes
606 and $CD11b^+CD45^{lo}$ microglia. Data are representative of three independent experiments.

607 Each point represents an individual animal. P values were determined by One-way ANOVA
608 with Tukey's post hoc test. dpi, days post immunization; F, females; M, males; *KO*,
609 knockout; Prog, progression.

610

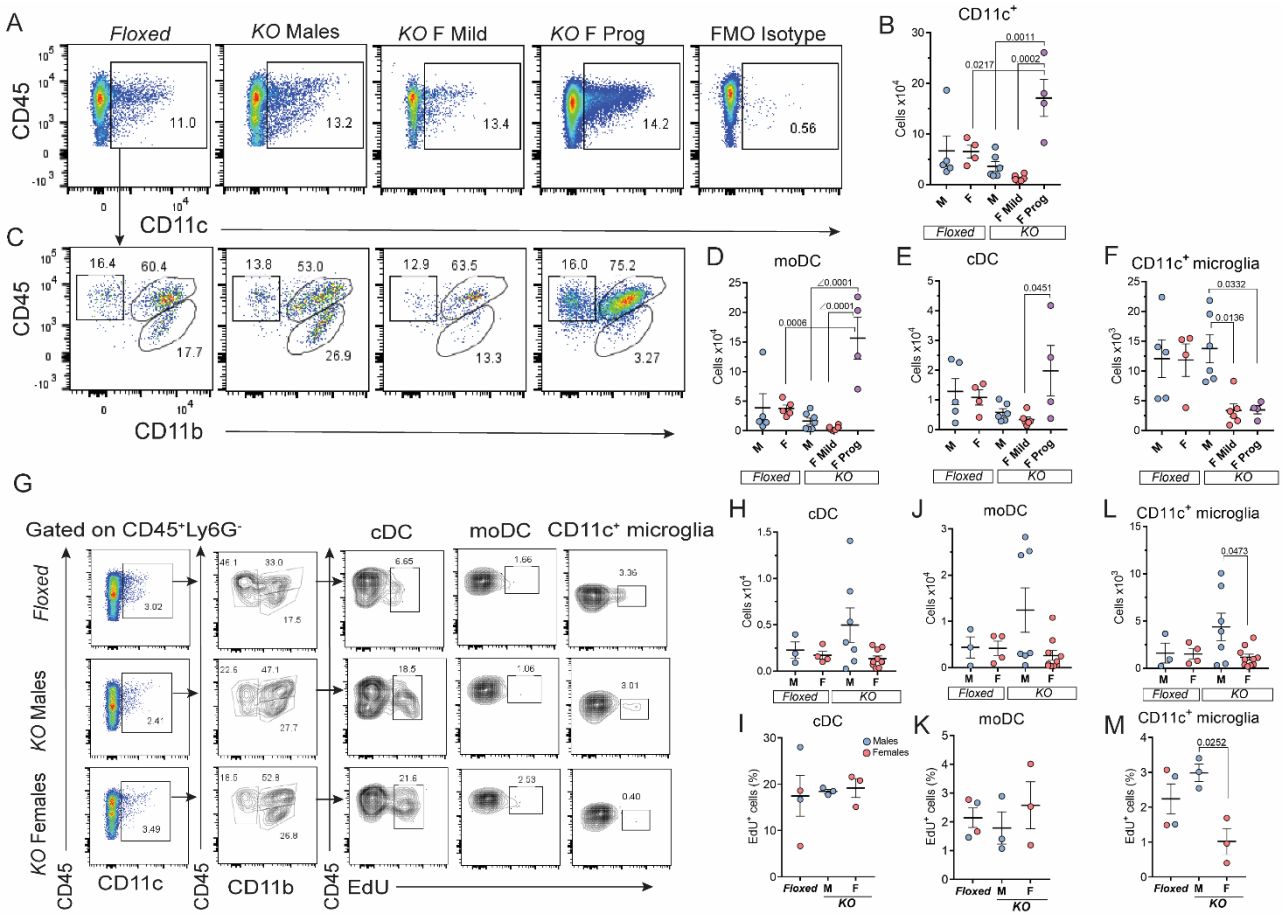

Fig. 2. Reduction in CD11c⁺ microglia at EAE progression in *KO* female mice. (A) Flow cytometry analysis of CD11c⁺ cells isolated from the brain and spinal cord of *Floxed* and *KO* male and female mice at 30 dpi. (B) Quantification of CD11c⁺ cells. (C) Flow cytometry analysis of cDC, moDC and CD11c⁺ microglia differentiated by expression of CD45 and CD11b. (D-F) Quantification of moDC, cDC, and CD11c⁺ microglia. (G) MOG-PTX immunized *p38α Floxed* control and CD11c promoter-driven *KO* female and male mice without EAE clinical symptoms at 30 dpi were injected with 12 mg/kg EdU twice in 12 h interval. EdU⁺ cells were analyzed 24 h after first injection. Proliferative response was determined as percentage of EdU⁺ cells of cell population. (H) Quantification of cDC. (I) Proliferative response of cDC. (J) Quantification of moDC. (K) Proliferative response of moDC. (L) Quantification of CD11c⁺ microglia. (M) Proliferative response of CD11c⁺ microglia. Data are representative of three independent experiments on immune cell quantification and two independent experiments on proliferative response. Each point represents an individual animal. *P* values were determined by One-way ANOVA with Tukey's post hoc test. dpi, days post immunization; F, females; *KO*, knockout; M, males; Prog, progression.

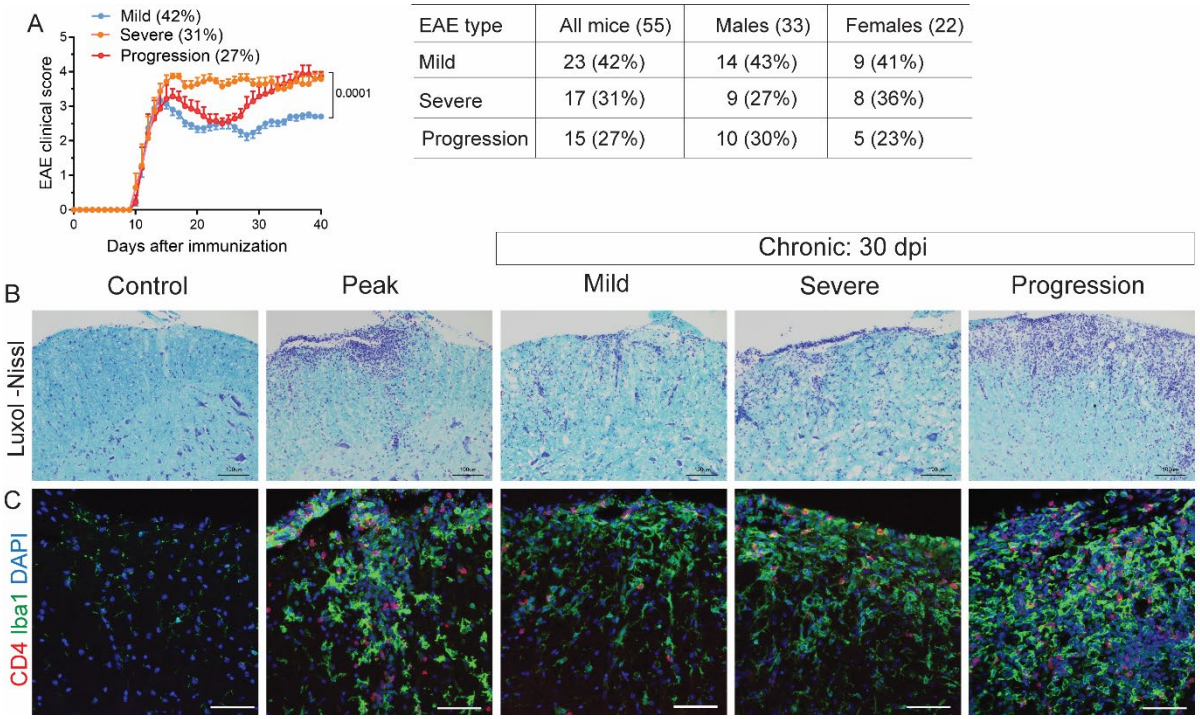

EAE type	All mice (55)	Males (33)	Females (22)
Mild	23 (42%)	14 (43%)	9 (41%)
Severe	17 (31%)	9 (27%)	8 (36%)
Progression	15 (27%)	10 (30%)	5 (23%)

Fig. 3. Diffuse parenchymal infiltration at EAE progression in *WT* mice.
EAE was induced in C57BL/6 mice with MOG prepared by syringe homogenization. (A) At 30 dpi animals were grouped based on EAE course: mild, severe or progression. Data are representative of six independent experiments. Individual time points represent mean ± s.e.m. *P* values were determined by two-way ANOVA with Sidak's multiple comparisons test. (B) Representative images showing demyelination and infiltration in the lumbar spinal cord of healthy control, at EAE peak, and in chronic mild, severe and progressive EAE. (C) $CD4^+$ T cells and $Iba1^+$ macrophages/microglia in the lumbar spinal cord of healthy control, at EAE peak, and in chronic mild, severe and progressive EAE. Scale bar 100 µm for Luxol-Nissl and 50 µm for CD4/Iba1. dpi, days post immunization.

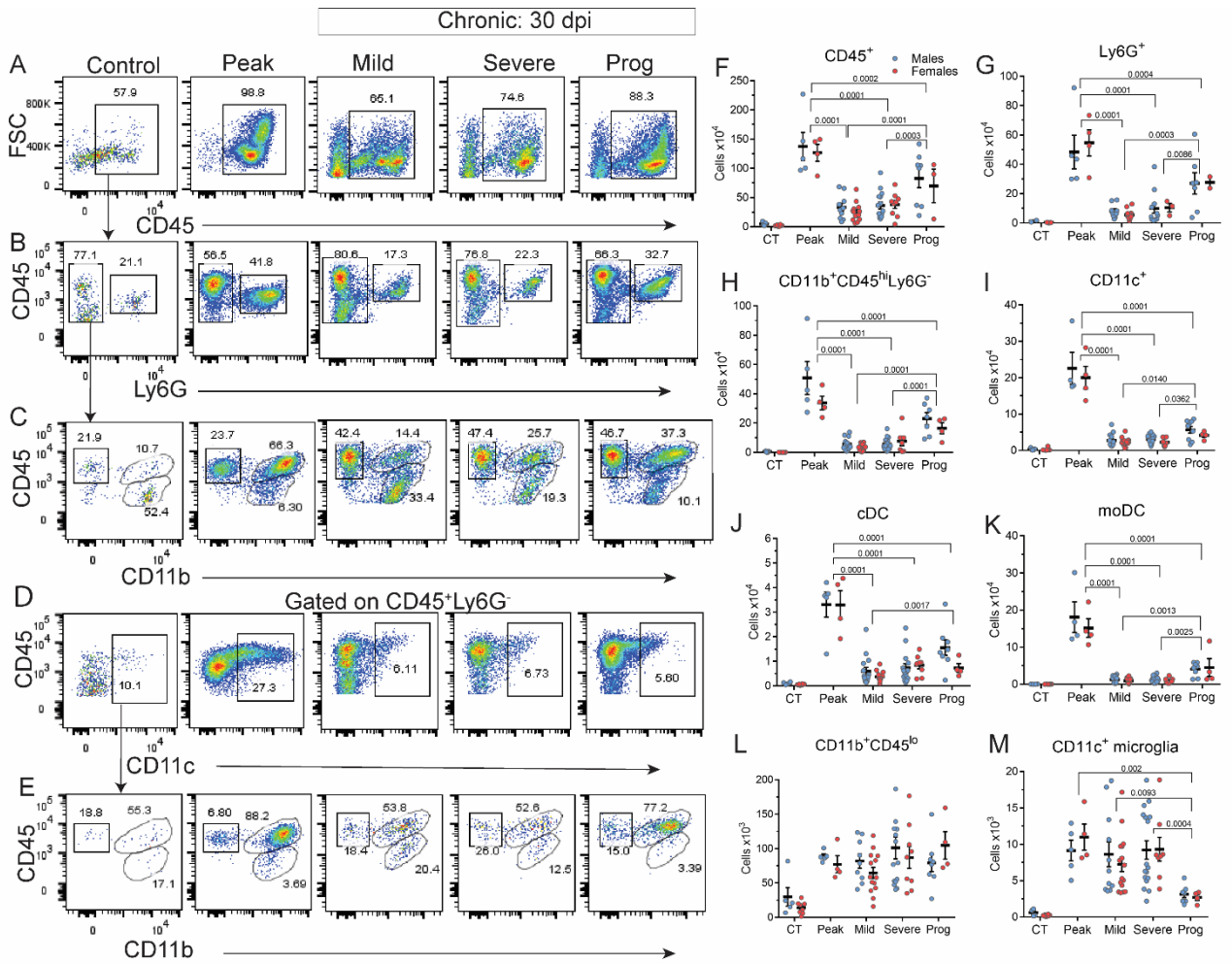

Fig. 4. Reduction in CD11c⁺ microglia at EAE progression in *WT* mice.
EAE was induced in C57BL/6 *WT* mice with MOG prepared by syringe homogenization. Flow cytometry analysis of cells isolated from the brain and spinal cord of healthy mice, at EAE peak, EAE progression and at 30 days of mild and severe EAE. (A-D) Flow cytometry analysis of $CD45^+$ cells, $Ly6G^+$ neutrophils, $CD11b^+CD45^{hi}Ly6G^-$ macrophages/monocytes and $CD11b^+CD45^{lo}$ microglia, $CD11c^+$ cells. (E) Gating strategy to differentiate cDC, moDC and $CD11c^+$ microglia by expression of CD45 and CD11b. (F-M) Quantification of $CD45^+$ cells, $Ly6G^+$ neutrophils, $CD11b^+CD45^{hi}$ macrophages/monocytes, $CD11c^+$ cells, cDC, moDC, $CD11b^+CD45^{lo}$ microglia, and $CD11c^+$ microglia. Data are representative of six independent experiments. Each point represents an individual animal. *P* values were determined by One-way ANOVA with Tukey's post hoc test. dpi, days post immunization.

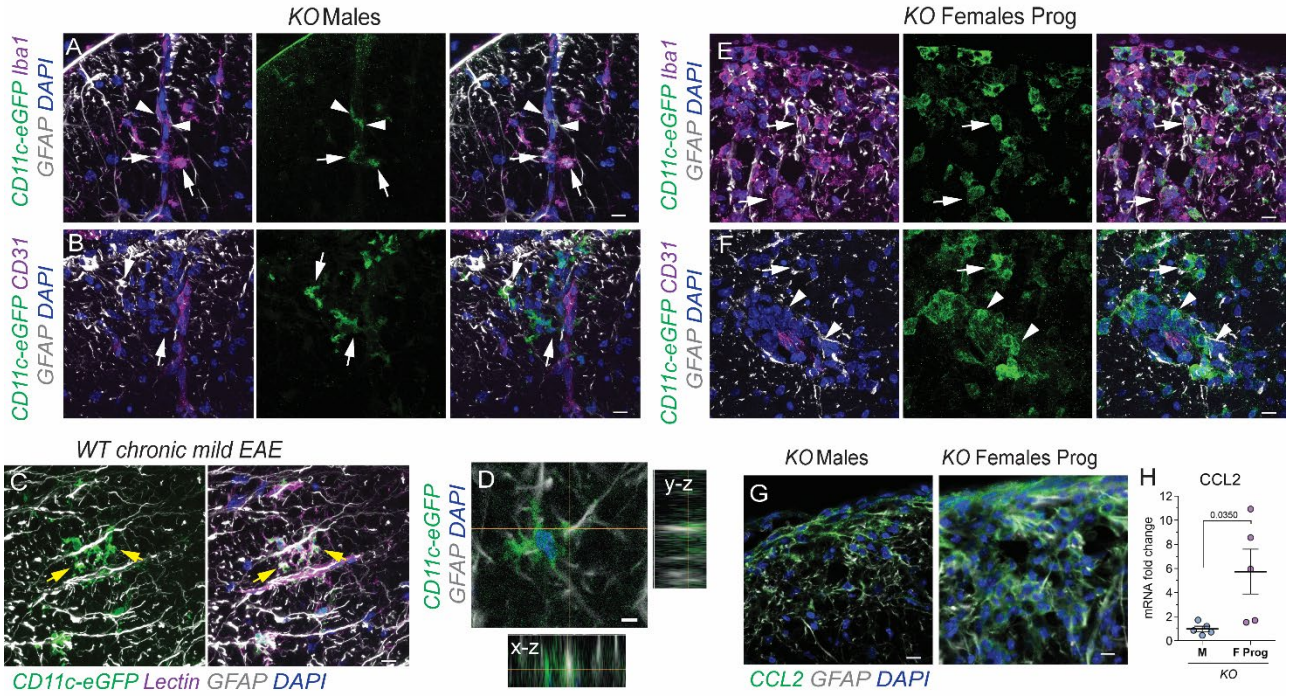

Fig. 5. CD11c⁺ microglia form contacts with astrocytes at the glia limitans. CD11c⁺ cells were visualized using CD11c promoter-driven expression of eGFP. (A-B) In the spinal cord white matter of protected *KO* males, parenchymal and perivascular astrocytes were surrounded by CD11c-eGFP⁺ microglia (arrows). moDC (arrowheads) were trapped within perivascular spaces. (C) CD11c⁺ microglia in contact with parenchymal astrocyte processes and glia limitans covering Lectin⁺ blood vessel (arrows) in *WT Itgax*-cre-EGFP mice in chronic mild EAE. (D) Orthogonal projection shows that dendritic-like CD11c⁺ microglia form contacts with astrocyte processes. (E) CD11c-eGFP⁺ moDC/reactive microglia surround hypertrophic processes of reactive astrocytes in the ventral spinal cord of progressed *KO* female mice (arrows). (F) moDC in the perivascular space (arrowheads) and parenchyma (arrows). (G) Increased CCL2 expression in reactive astrocytes in progressed *KO* females. Scale bars 10 µm for A-B, D-G and 5 µm for C. (G) mRNA transcription levels of CCL2 in the lumbar spinal cords of *KO* male and progressed *KO* female mice. Data are representative of three independent experiments. Each point represents one individual animal. P values were determined by Student's t-test. F, females; *KO*, knockout; M, males; Prog, progression.